Neogene-Recent Reactivation of Jurassic-age Faults in Southern Vietnam, with Implications for the Extrusion of Indochina

Authors: CM Burberry[1]*, LJ Elkins[1], Nguyen Hoang[2], Le Duc Anh[2], Sang Q. Dinh[3].

Affiliations: [1]UNL, Lincoln, Nebraska [2]VAST, Hanoi, Vietnam, [3]Petrovietnam University, Vietnam

*cburberry2@unl.edu

ABSTRACT

Onshore Vietnam contains a complex series of faults coupled with a diffuse igneous province that has been active since the mid-Miocene. However, there are several conflicting fault maps in the literature and no consensus concerning the relative age of mapped faults and Neogene basalt flows, which becomes problematic when trying to use structural data to distinguish between competing tectonic models for the SE Asia region. This paper aims to define the Neogene-Recent tectonic setting and kinematics of the Da Lat block of the onshore Vietnam region, by analyzing the orientation, kinematics and ages of faults across a sub-region of the block. Fault ages can be constrained by the cross-cutting relationships with dated basalt flows. Results from remote sensing show a strong NE-SW fault trend for southern Vietnam, with additional, minor N-S, E-W and NW-SE trends. Fault orientations observed in the field fall into this NE-SW trending class, and are sub-vertical. In the basalt flows (with eruption ages < 5 Ma) these faults have oblique lineations with a strong strike-slip component. In Jurassic sediments, these faults show two sets of lineations: an older, dip-slip set, and a younger, oblique-slip set. We postulate that Jurassic-age dip-slip faults have been reactivated as strike-slip faults post 5 Ma. Strike-slip motion on NE-SW oriented faults is consistent with rotation and extrusion of the Kontum and Da Lat blocks. Rotation of the blocks is

consistent with continuum rubble behavior of small crustal blocks under the influence of extrusion-driven asthenospheric flow.

Keywords: Vietnam, Indochina, tectonic extrusion, block rotation, strike-slip faults, fault reactivation

1. Introduction

Onshore Vietnam is a complex region of faulting coupled with a diffuse igneous province that has been active since the mid-Miocene (Figure 1a, b). However, there is no agreement over the relative ages of mapped faults and known volcanic centers, as there are several conflicting fault maps and interpretations of present-day fault activity (e.g. Huchon et al., 1994a; Rangin et al., 1995; Figure 2) for the southern Vietnamese region. This lack of consensus over relative age becomes problematic when trying to use structural data to distinguish between the two competing tectonic models for the evolution of southern Vietnam, that of extrusion tectonics related to the collision of India with Eurasia, which is thought to have ceased at ~5 Ma (Leloup et al., 2001; Zhu et al., 2009), or that of far-field extension related to past spreading in the South China Sea region which ceased at ~16 Ma (e.g. Li et al., 2015). Onshore Vietnam is also characterized by complex stress fields and absolute motions (Michel et al., 2001; Simons et al., 2007; Tingay et al., 2010; Tran et al., 2013) which cannot easily be explained if the region is a coherent part of the stable Sundaland block (Tingay et al., 2010).

The first model considered here is that of “extrusion” or “escape” tectonics, the process by which the collision of two tectonic blocks leads to lateral escape of material formerly located between those blocks. Extrusion has also been invoked to explain the evolution of areas including Alaska and the Anatolian block in Turkey (Finzel et al., 2011; Gursoy et al., 1997, 2003; Mantovani et al., 2002; Redfield

et al., 2007; Ridgeway and Flesch, 2007; Tapponier et al., 1986). The mechanisms behind extrusion tectonics remain poorly constrained, however. The proposed extrusion model for Indochina (see e.g. Chamot-Rooke and Le Pichon, 1999; Chi and Dorobek, 2004; Chi and Geissman, 2013; Flower et al., 1998; Hoang and Flower, 1998; Michel et al., 2001; Morley, 2007; Tingay et al., 2010; Yan et al., 2006) posits that 1) strong coupling between the asthenosphere and lithosphere and a significant mantle drag torque has translated the Southern Indochina microplate in response to extrusion of asthenosphere by the closure of the Tethys Sea and Himalayan collision; and 2) the extruded lithospheric block is characterized by giant strike-slip faults, smaller scale strike-slip faults and pull-apart basins, and minor normal faulting.

Seismic interpretation from two basins offshore from southern Vietnam, however, indicates a phase of rifting coeval with the propagation of the South China Sea rift zone, and ascribes the presence of the more recent faulting and onshore diffuse volcanic activity purely to the westward propagation of this rift and associated thermal subsidence (Fyhn et al., 2009a, b). These data suggest that normal faulting off-shore predates the voluminous volcanism onshore, and suggests that the volcanic flows erupt into existing rift or pull-apart basins (Huchon et al., 1994b). However, South China Sea spreading ceased about 16 Ma (Li et al., 2015), and it is unclear whether far-field thermal subsidence can induce fault activity. The extension-dominated model is expected to produce faults that 1) either pre-date or are synchronous with volcanic activity, but do not post-date volcanic activity; and 2) have a dominant sense of motion that is normal.

As noted above, existing fault maps are inconclusive (e.g. Huchon et al., 1994a; Rangin et al., 1995; Figure 2) as to the age relationships between faulting and the basalts of the diffuse igneous province. These maps are also inconsistent with respect to the sense of motion on the mapped faults (e.g. Searle et al., 2010; Zhu et al., 2009), making it difficult to reconcile the tectonics of the region with either of the two models proposed above. The scenario is further complicated by the recognition by local workers (e.g. Kasatkin et al., 2017) of major strike-slip faults within the Indochina block that dissect southern Vietnam,

forming the Da Lat and associated blocks (Figure 1b), and suspected to be lithospheric in scale. This paper aims to define the Neogene-Recent tectonic setting and kinematics of the Da Lat block of the onshore Vietnam region, by analyzing the orientation, kinematics and ages of faults across a sub-region of the block. Fault ages can be constrained by the cross-cutting relationships with dated basalt flows. These results are used to demonstrate that there has been Cenozoic fault activity in the Da Lat block of southern Vietnam that (a) post-dates the activity in the diffuse igneous province, (b) potentially reactivates older faults, (c) is more consistent with an extrusion-based tectonic history than an extension-based tectonic history for the region, and (d) has implications for how extrusion may be accommodated once a free surface is no longer present.

2. GEOLOGIC SETTING

A series of structural, tectonic, and geophysical lines of evidence have been put forward to support tectonic extrusion as the key driver of tectonic and volcanic activity in Indochina. That evidence includes the presence of large-scale transform faults such as the Red River Fault Zone (linked to the East Vietnam Transfer Zone) and the Mae Ping Fault Zone. The pattern of these major strike-slip faults in Southeast Asia is markedly similar to the pattern of large-scale, left-lateral strike slip faults generated in analog experiments by Tapponier et al. (1982, 1986). These experiments assume that the western Pacific is acting as a free surface, that Greater India acts as a rigid indentor, and that Eurasia is segmented and extruded toward the free surface in order to accommodate the collision. For example, the Red River fault zone separates the South China block from the Indochina block, and showed left-lateral movement for much of its history (Rangin et al., 1995). The extrusion model for Indochina further assumes a component of mantle flow roughly parallel to the strike of the major faults (e.g., Flower et al., 1998; Hoang and Flower, 1998; Yan et al., 2006), which is corroborated by anisotropy recorded in shear-wave splitting data for the

upper mantle beneath the northern part of the Indochina-Shan Tai complex (Bai et al., 2009). Paleomagnetic and GPS data suggest that the lithosphere is broken into a series of rigid blocks, where the Kontum and associated blocks may be moving eastwards and rotating, and the Shan Tai block may be rotating and moving to the south (Chamot-Rooke and Le Pichon, 1999; Chi and Dorobek, 2004; Chi and Geissman, 2013; Michel et al., 2001; Morley, 2007; Tingay et al., 2010). One major challenge to the extrusion model is that left-lateral motion along the Red River fault zone, a key signature of extrusion of Indochina, ceased around 17 Ma, and became right-lateral motion by 5.5 Ma (e.g., Leloup et al., 2001; Zhu et al., 2009). This cessation of left-lateral movement is frequently considered to mark the end of extrusion of the Indochina block, but may instead mark a change in regional or local kinematics. Coeval with the change in motion is inversion of some of the northern-most basins along the Red River Fault Zone, such as the Song Hong Basin (Fyhn et al., 2018). Inversion can also be noted in Cuu Long and Nam Con Son basins of south Vietnam (Pubellier & Morley, 2014). The cause of this change in plate kinematics is variously ascribed to the ridge jump in the SCS, a change in Indian indentor motion (e.g. coupling the Indian and Burmese blocks; Fyhn et al., 2009a, b), or an additional plate tectonic reconfiguration in the region such as the collision of Australian fragments to the SE of Sundaland (Pubellier & Morley, 2014).

Extensional tectonics in Indochina have been well documented, starting with Jurassic-Cretaceous age back-arc rifting, due to the subduction of the proto-Pacific crust under Vietnam, Borneo and South China (Nam, 1995; Morley, 2012). Jurassic-Cretaceous rift locations were partially influenced by weak zones resulting from the Indosinian Orogeny, the collision of the Sibumasu, South China and Indochina blocks during the Triassic (Lepvrier et al., 2004; Pubellier & Morley, 2014). The Jurassic-Cretaceous event was initially followed by Late Cretaceous rifting along the proto-South China basin (Barckhausen et al., 2014; Chung et al., 1997; Zhou et al., 1995) and subsequently by the opening of the SCS, which experienced ocean spreading from 32 Ma. Spreading either ceased at 20.5 Ma (Barckhausen et al., 2014) or at 16 Ma for the southwest sub-basin of the SCS, closest to our study area (Li et al., 2015). After SCS spreading

ceased, rifting may have propagated onshore, while lingering upper mantle upwelling generated ongoing diffuse seamount activity within the SCS (Barckhausen et al., 2014; Cullen et al., 2010; Matthews et al., 1997; Swiecicki & Maynard, 2009; Yan et al., 2006). The date of 16 Ma also corresponds with the change in motion along the Red River fault zone described above, marking a change in regional plate kinematics. Regional compression and uplift led to widespread erosion across southern Indochina during the Paleocene, with the development of significant unconformities across southern Indochina (Fyhn et al., 2009a; Tri et al., 2011).

After the cessation of SCS rifting, regional uplift rates also became more rapid, contemporaneous with the initiation of onshore volcanism in the Miocene (Carter et al., 2000; Fyhn et al., 2009a; Wang et al., 2006). Onshore, eruptions of basalt have occurred in four significant phases since the Miocene: 17-12 Ma, 9-7.4 Ma, 5.4-1.75 Ma and 0.7-0.57 Ma (Tri et al., 2011). Fyhn et al. (2009a, b), Cullen et al. (2010) and Savva et al. (2013) asserted that the observed patterns of uplift and on- and offshore volcanism are purely the product of regionally propagating extension following the cessation of oceanic rifting, though they do not otherwise explicitly account for the large volume of onshore volcanics. All sets of work produced seismic lines across the offshore Phu Khanh, Cuu Long, and Nam Con Song basins and interpret two to three stages of rifting, separated by a period of tectonic quiescence. Crucially, the last rifting phase is after the cessation of active SCS spreading (Matthews et al., 1997; Swiecicki & Maynard, 2009; Savva et al., 2013). In the Phu Khanh basin, rifting is interpreted to be transtensional and related to the offshore trace of the Red River Fault Zone (Fyhn et al., 2009a, b; Cullen et al., 2010; Savva et al., 2013). Rifting in the Cuu Long and Nam Con Song basins is interpreted by these authors to be related to continued regional extension associated with SCS extension, even though active spreading to the east has ceased (Matthews et al, 1997; Fyhn et al., 2009a, b; Dung et al., 2018). Volcanic eruptions there appear to have been emplaced along fault planes, suggesting rifting predates volcanic activity (Fyhn et al., 2009 a, b), but it is

not clear if this pattern continues onshore, where the major tectonic regime during the Pliocene-Holocene is thought to be thermal subsidence (Tri et al., 2011).

There are thus a number of observations that are not well explained by an extensional tectonic model for southern Vietnam, such as the ongoing and voluminous volcanism, the origins of offshore rifting after SCS spreading ended, and the change in fault motion of the Red River fault. Using fault geometries and timing, palinspastic reconstructions, and geophysical data, some workers have thus instead attempted to reconcile the extrusion model of Indochina with the opening of the SCS. The end-member models state that SCS rifting is completely independent of the extrusion of Indochina (e.g., Chung et al., 1997; Clift et al., 2008; Yan et al., 2006), or that the opening of the SCS basin is a direct consequence of the stress regime imposed by the extrusion of Indochina (e.g., Briais et al., 1993). Zhou et al. (1995) and Fyhn et al. (2009a) propose that extrusion tectonics had some effect on ridge axial relocations in the SCS as noted by Briais et al. (1993), but that initial opening of the basin was independent of the India-Himalaya collision. Cullen et al. (2010) propose that neither slab rollback in the western Pacific, nor extrusion of Indochina can fully explain the tectonic setting of southern Vietnam, and invoke additional asthenospheric upwelling to provide sufficient crustal extension, heat flow, and volcanism. Seismic data support the presence of a shallow mantle thermal anomaly underlying Indochina, which may reflect diffuse mantle upwelling in support of dispersed volcanic activity (Liu et al., 2004), and the region has documented high heat flow (Duchkov et al., 1992; Uyeda, 1994).

Further, GPS data, albeit a sparse dataset, indicates that the Sunda block moves as a rigid and coherent unit, with an absolute motion to the ESE (Michel et al., 2001; Simons et al., 2007; Tran et al., 2013). However, the stress field across the Sunda block is heterogeneous, rather than subparallel to the absolute motion vector (Tingay et al., 2010; Van Nquyen & Hoai, 2019) suggesting that the question of whether this region can best be described in terms of block tectonics or continuous deformation (Calais et al., 2006) is unresolved. In the case of Indochina, the block tectonics hypothesis of Calais et al. (2006)

is potentially compatible with an extrusion-driven origin for Neogene-Recent deformation in the region, whereas the continuous deformation field hypothesis is more compatible with regional stretching and thermal subsidence related to South China Sea rifting.

Existing data shows other discrepancies in the Da Lat and surrounding blocks (Figure 1b, 2), where previously generated remote sensing and field focused maps (e.g. Huchon et al., 1994a; Rangin et al., 1995) do not agree on fault locations or trajectories, nor on whether faults cut the voluminous basalt flows or whether the flows overrun the major faults. Van Nguyen & Hoai (2019) provide several data points where faults are observed to cut the Neogene or Quaternary basalts, although the bulk of their data points are in the Cretaceous age granites. Studies of basalt flow ages (e.g. An et al. 2017; Lee et al. 1998) show that many of the flows in the Da Lat block are significantly younger than 5 Ma, indicating that volcanism and potentially faulting are ongoing in the study area.

3. METHODS

This study was a joint remote-sensing and field study. We interpreted lineaments across the field area, using both Landsat ETM+ data and SPOT data. Figure 3 shows Landsat ETM+ and SPOT coverages, together with field locations. Landsat ETM+ datasets were sourced from the Global Land Cover Facility (GLCF) and the SPOT data were sourced from Apollo Mapping. Landsat ETM+ data were downloaded as separate bands and combined into a false color composite. Bands 531 were combined as RGB in ArcGIS. This raster was stretched using the histogram equalize operation. Landsat ETM+ data were also combined as a true color composite using bands 321 as RGB in ArcGIS. This imagery was blended using a standard deviation stretch. SPOT data was provided as a true color composite by the vendor. The data were already georeferenced to the Landsat ETM+ reference frame. Digital Elevation Model (DEM) data were also sourced from the GLCF and displayed as classified datasets in ArcGIS. As for the Landsat ETM+ datasets,

186 the interactive map tool was used to define the study area and locate the datasets. The remote datasets
187 were compiled into an ArcGIS project and the field locations and other information were added by
188 database upload or by georeferencing jpg files. Other information comprises: 1) maps from Huchon et al.
189 (1994a), Rangin et al. (1995), and the Department of Geology and Minerals, Vietnam; and 2) locations
190 with dated basalt samples from Lee et al. (1998) and An et al. (2017).

191 Lineaments were picked from the satellite maps on the basis of textural changes in the images, or by
192 considering the changes in stream patterns. For example, abrupt changes in direction of stream channels,
193 or abnormally straight segments of streams, indicate the presence of joints or faults in the subsurface
194 governing that stream pattern (Drury, 2004). In addition, linear changes in texture of the land surface
195 often indicate a fault-controlled change, although care must be taken to avoid regions where the land
196 surface has been altered by humans. Such regions can be identified by the typical regular checkerboard
197 pattern of cultivated fields and field boundaries and the proximity to dwellings. It should be noted that
198 there are two resolutions of data in the imagery and thus there will be areas where lineaments may be
199 more densely picked than others; in addition, there are regions of the study area that are densely
200 populated and cultivated, such that there is not an even coverage of lineaments across the study area.
201 Once picked, the lineament map was classified using the ArcGIS Grouping Analysis algorithm, nearest
202 neighbor option, within ArcGIS. The lineaments were classified into 50, 75 and 100 bins, and the 75-bin
203 option was used to compare the lineaments to the field dataset and known earthquake locations in order
204 to produce a predicted deep-seated fault map of the area. The predicted deep-seated faults were picked
205 based on dominant orientation within the lineament clusters. The 75-bin option was used because, on
206 inspection, this option did not split trends that were apparent from the satellite data, which the 100-bin
207 option was prone to doing. The 50-bin option gave clusters that were too coarse when compared to the
208 field dataset.

We also undertook a reconnaissance field trip in 2016 to the southern part of the Central Highlands, near Ho Chi Minh City, Buon Ma Thuot, and Vung Tau. We observed lithology at every stop, and where relevant, we took measurements of bedding attitude, fault attitude and fault lineation pitch within the fault plane. At each site, we noted the relationship of faults and the host lithology, considering whether the fault terminated against lithological elements, or cut all observable lithologies. On our return to the lab, these data were synthesized using GIS and Stereonet 10™ to determine similarity in fault orientations, possible fault kinematics and the relationship to the lineament map.

To clarify the age of structural elements, the age of one alkali basalt flow (field sample number 2016-CH-10, retrieved from location 10.5076ºN, 107.2729ºE, and 229 ft. elevation), was determined using $^{40}Ar/^{39}Ar$ methods at the Oregon State University Argon Geochronology Lab in Corvallis, Oregon. The sample was crushed, sieved to ~300 μm grain size, rinsed in distilled water and dried at low temperature in an oven (~80ºC), then mildly leached to remove impurities. The procedure for leaching was a 20 min. soak in 5% HNO_3 in an ultrasonic bath, followed by 3 rinses in distilled water, then a 20 min. soak in distilled water in the ultrasonic bath and 3 more distilled water rinses; the sample was then again dried at 80ºC or lower in the oven. Following this preparation procedure, the sample was irradiated in the TRIGA experimental reactor at the OSU Radiation Center at 1 MW power. The neutron flux during irradiation was monitored using the FCT-NM standard, with an adopted age of 28.20 ± 0.02 Ma (after Kuiper et al., 2008), and a $^{40}Ar/^{39}Ar$ = 9.733 ± 0.008 and J-value of 0.001615 ± 0.000001. For mass spectrometry, the sample was analyzed by incremental heating using a bulk CO_2 laser heating method on the ARGUS-VI-D instrument at OSU. Ages were determined using a decay constant of 5.53 ± 0.05 x 10^{-10} a^{-1} (Steiger and Jäger, 1977) using age correction methods after Min et al. (2000). Heating plateau ages were determined using an error weighted mean of plateau steps. Additional standard and procedural blank results are available in the Supplementary Information.

4. RESULTS

4.1 Remote sensing

Figure S1 shows lineament orientations mapped via remote sensing across the study area. In total, 2323 lineaments were picked across the study area using the methods described above. Figure S2 shows a rose diagram of those lineament orientations, and shows a strong N-S to NE-SW fault trend, with very minor components in other cardinal directions. 11.7% of the data is distributed between a bearing of 031 and 040. Figure 4 shows the classified lineaments, which were classified using the ArcGIS algorithm as described above, and each cluster is shown in a different color. Note that there is a strong preferred orientation within many of these clusters. For example, in the NW of the study area and to the W of the lake, there is a teal-colored cluster which trends NNE-SSW. These lineaments all cut basalt flows which have been previously dated as 4.3+/- 0.2 Ma (An et al. 2017) or ranging between 2.42+/- 0.08 Ma (south of Xuan Loc center) to 0.24 +/- 0.06 Ma (north of Xuan Loc center; Lee et al., 1998; Figure 5) and thus fall within the second youngest and youngest phases of basalt extrusion. Figure 5 further shows that the lineaments do not preferentially cut basalts or clastic units, but are distributed between the Jurassic to Quaternary formations without an apparent skew to one type of formation.

These data imply that there is a strong lineament orientation trending NE-SW across the study area and that is in many cases younger than 4.3 +/- 0.2 Ma (An et al. 2017). Below we compare the lineament data with the field data to further assess the nature of these lineaments.

4.2 Field data

Here we describe field observations for a series of sites across the study area (Table 1, Figure 3), in order of observation. All strike and dip data is expressed using the Right Hand Rule convention, so no dip quadrant is listed.

At location 1 (Figure 3), a series of faults cutting Jurassic sediments were observed (Figure 6). One key fault (Figure 6a, b) had an attitude of 024/88 with two sets of lineations, one pitching 16°SW and the other pitching 80°SW (Figure 6c). Figure 8b shows that the sub-horizontal lineation cross-cuts the dip-slip lineation on this fault surface. On the other side of the same quarry, faults were observed with attitudes of 027/58 (dip-slip lineations) and 015/48 (no visible lineations) (Figure 6c). We could not identify whether the oblique slip lineaments were left-lateral or right-lateral as there were no identifiable "steps" in these lineaments.

At location 2 (Figure 3), a series of faults cutting the Soc Lu Formation were observed (e.g. Figure 7a). The Soc Lu Formation at this locality has been dated to 4.3 +/- 0.2 Ma (An et al., 2017). Field observations of plagioclase and biotite phenocrysts in Soc Lu volcanics suggest that the Soc Lu Formation eruptives include basaltic andesite, and the observed flow coverage (not shown in Figure 5 due to its limited extent) suggests a relatively small flow unit within the Xuan Loc volcanic center. The faults at this location strike NE-SW and are sub-vertical. One fault has an attitude of 036/76 and two other fault surfaces are oriented 023/85 and 028/80. On each fault surface, sub-horizontal lineations were observed, with pitches of 12°NE, 12°NE and 18°NE respectively (Figure 7b). Again, we were not able to discern whether the lineations gave a sense of left- or right-lateral movement because convincing "steps" in the lineations were not identifiable on these fault planes.

At location 3 (Figure 3), an old quarry in the alkali basalts of the Xuan Loc Formation where mantle xenoliths were observed, additional faults were observed with orientations of 172/57 and 121/80. The first of these faults was marked by heavily foliated basalt, and neither fault displayed lineations.

Locations 4-7 are clustered close together in faulted Cretaceous age granites near Vung Tau. These granites are part of the Deo Ca complex which has been dated at either 88-92 Ma or c. 118 Ma by U-Pb zircon geochronology (Ngyuen et al. 2004; Shellnutt et al., 2013; Hennig et al., 2018). One major fault with

several strands and a damage zone of tens of cm wide has an attitude of 236/84 (Figure S3a). Other fault surfaces have attitudes of 228/74 and 294/76, and these fault zones contain black material that may be pseudo-tachylite or later intruded and sheared mafic material (Figure S3b). The major fault zone oriented at 236/84 corresponds to the known Ca Na-Vung Tau fault zone (Figure 1b) which bounds the Da Lat block to the south.

At location 8, an alkali basalt quarry north of Vung Tau, a series of joints were measured, as there was no visible evidence of faulting on the safely accessible exposed faces of this active quarry. The pole figure for this dataset is found in Figure S4. A strong cluster of poles is found marking a joint set oriented ENE-WSW, amongst a near uniform distribution of other joints. We infer that this outcrop was cut by a combination of columnar, i.e. basaltic cooling joints, and a systematic set of joints oriented ENE-WSW.

Sample 2016-CH-10 from location 8 was determined using $^{40}Ar/^{39}Ar$ age dating methods to have an initial eruption age of 0.600 ± 0.004 Ma (2σ). This weighted mean plateau age is consistent with ages calculated using the alternative total fusion (0.599 ± 4 Ma), normal isochron (0.599 ± 0.006 Ma), and inverse isochron methods (0.599 ± 0.006 Ma) (see Supplementary Information for additional raw data and plateau age results for this analysis). The mean squared weighted deviation for the plateau age is 0.002 Ma, and calculated K/Ca ratio is 0.21 ± 0.09 (2σ).

These data indicate that there are small-scale faults and fractures that both pre and post-date the basalt flows across the studied area of the Da Lat block. The following section will compare this dataset to the lineament dataset and derive a model for the generation of the small-scale faults and fractures.

4.3 Combining the datasets

The small-scale faults and fractures of the field dataset are overall interpreted to be the classified lineaments of the remote sensing dataset. However, some of the faults in the field dataset predate the basalts while others post-date the basalts. In addition, at Location 1, the fault in the Jurassic-Cretaceous

sediments has been reactivated, indicating the occurrence of multiple events. We infer that the faults documented at Locations 1 and 4-7 with age constraints of either post-Jurassic or post-Cretaceous (that is, post c. 118 Ma or post 88-92 Ma) are deeper seated or pre-existing faults. These pre-existing faults predate Late Cretaceous and younger sedimentation and basalt effusion in the region. Such faults can be estimated from the average orientations of classified lineament clusters as shown in Figure 8. In some cases, additional data such as earthquake event locations were used to identify these deeper seated or pre-existing faults. We infer that many of these deeper and/or pre-existing faults initiated as rifts in the Jurassic or Cretaceous and have since been reactivated as strike-slip faults during later deformation. In some cases (e.g., Figure 9a, b) classic lineament patterns are observed that suggest reactivation of the deeper-seated fault as a transpressional flower structure.

4.4 Model for faulting across the Da Lat Block

Considering the faults at locations 1 and 2, we infer that the NE-SW trending faults cutting the basalt flows are genetically related to the NE-SW trending faults in the Jurassic sediments. We postulate that (a) the Jurassic-Cretaceous, steeply dipping dip-slip faults or joints have been reactivated as strike-slip faults during the Neogene (location 1), and (b) this reactivation of deeper-seated faults led to the generation of damage in the overlying Neogene basalts. This damage is manifested as the smaller-scale strike slip faults observed at location 2 and potentially as the fractures noted and measured at location 8, although we acknowledge that these fractures may be due to a different phase of relatively recent deformation within the Da Lat block. The development of strike-slip motion on faults oriented dominantly NE-SW within the Da Lat block is consistent with the continued extrusion of this block within the large-scale shear zone created by the Three Pagodas Fault and Ailo Shan-Red River-East Vietnam shear zones (Figure 1a). We therefore propose that extrusion did not cease at 5 Ma as has been previously suggested, but is ongoing, and is now accommodated by the rotation of blocks such as Da Lat and by internal deformation within this part of Sundaland. We speculate that the kinematics of the extrusion regime

changed with the change in regional plate dynamics, as discussed in Section 2, and with the effective removal of the Western Pacific free surface by the collision of Luconia, Dangerous Grounds and Reed Bank with NW Borneo and Palawan (Hall, 2002; Hall et al., 2008; Clift et al., 2008). In our conceptual model, the individual blocks shown in Figure 1b are moving semi-independently, similar to the continuum deformation style proposed by Calais et al. (2006). Under the existing extrusion model, Vietnam and the Da Lat block move to the SE (e.g. Tingay et al., 2010). Under our new model, the Da Lat block moves semi-independently to the SW to accommodate extrusion.

5. DISCUSSION

Contrary to existing literature (e.g. Rangin et al., 1995; Searle et al., 2010; Zhu et al., 2009) which states that faulting of both extrusion and extension regimes has ceased in the Indochina Peninsula, our results demonstrate that faulting has been more recent than 4.3 ± 0.2 Ma (An et al. 2017), 0.600 ± 0.004 (this study), or 0.24 ± 0.1 Ma (Lee et al., 1998). This is more recent than the postulated end of extrusion based on the change in motion of the Red River Fault Zone (5.5 Ma; Leloup et al., 2001; Zhu et al., 2009) and, significantly, the cessation of rifting in the South China Sea (16 Ma: Li et al, 2015). Thus, a tectonic regime more complex than thermal subsidence must be operating across onshore Vietnam, and we propose that this regime is extrusion-related. We do not favor the extension argument because the key faults observed at locations 1 and 2 were oriented NE-SW and showed oblique to strike-slip movement, whereas under an extensional regime, faults in this orientation would show oblique to dip-slip movement. Our proposed model of continuum block deformation of the onshore Vietnam region and southwestwards movement of the Da Lat block further predicts dominantly left-lateral movement on the NE-SW oriented strike-slip faults that were observed in the field and on the East Vietnam Transfer Zone (Trinh et al., 2015). While the lineations observed to-date do not show stepwise patterns that allow us to identify the sense

of motion to test this prediction, because we do not observe dip-slip motion on these faults we can still effectively rule out an extension-dominated regime related to the SCS. The presence of strike-slip faulting is compatible with the results from extensive field mapping in the Cretaceous granites reported by Van Nguyen and Hoai (2019). Van Nguyen and Hoai (2019) further reported four stress regimes operating since the end of the Oligocene and interpreted a rotation in the stress field associated with extrusion. We note that there is some spatial variation in each stress field across the Song Ba fault, which separates the Kontum and Da Lat blocks. Thus, we surmise that the Van Nguyen and Hoai (2019) dataset is compatible with our model.

We have generated a proposed pre-Neogene fault map (Figure 8) for a sub-region of the Da Lat block, based upon lineament mapping and cluster analysis, which is distinctly different from the fault maps generated by previous authors and shown in Figure 2. Our fault map has a denser distribution of structural features than the maps shown in Figure S5 and consists of shorter discrete fault segments, due to improved imagery resolution. Our fault map is also unique in that it constrains the ages of the remotely sensed faults (post-Jurassic and pre-Neogene, i.e. pre-basalt effusion) and distinguishes these older, deeper-seated faults from the more recent, smaller-scale faults and fractures visible on the lineament map that cut Neogene-Recent basalt flows. We further suggest that the older structures (Figure 8) date from late Jurassic subduction under the leading edge of the Kontum block and contemporaneous, associated intraplate extension, as documented by Tri and Bao (2011). An episode of basin inversion may have reactivated these faults in the late Miocene-early Pliocene (Tri and Bao, 2011) due to a change in direction of Indian plate subduction, coincident with the change in sense of motion of the Red River Fault Zone (e.g., Leloup et al., 2001; Zhu et al., 2009).

The Red River Fault Zone ceased left lateral motion around 17 Ma and initiated right-lateral motion approximately 5.5 Ma (e.g., Leloup et al., 2001; Zhu et al., 2009; Zuchiewicz et al., 2013). As noted above, this change was previously inferred to mark the end of extrusion of Indochina, but instead we

suggest that this marks a change in the kinematics of the extrusion process. During right-lateral motion, the major block being extruded is the South China block (Guo et al., 2001; Meng et al., 2005). However, this does not account for asthenospheric flow associated with the extrusion of Indochina, or for documented ongoing volcanism (e.g., the 1923 eruption of Ile des Cendres), which suggests continued mantle flow and upwelling (e.g. Hoang and Flower, 1998). To accommodate the motion of the mantle conveyor belt beneath, the Shan Tai, Kontum, Da Lat and other blocks would need to rotate within the confines of the larger scale shear zone defined by the Red-River – East Vietnam Transform and the Mae Ping Fault Zones. This is required because there is no free surface into which these blocks can be extruded, given their position in the core region of Sundaland. This suggestion posits a strong coupling between the asthenosphere and the lithospheric blocks in this area, in contrast to the relatively weak mantle drag torque inferred for areas with high subduction zone torques (e.g., the Nazca and Pacific plates; Chapple & Tullis, 1977). We therefore suggest that extrusion tectonics require a strong lithosphere-asthenosphere coupling, and that once the free surface is removed by other tectonic processes, block rotation is the inevitable consequence of ongoing mantle flow.

Paleomagnetic and GPS data from the core of Sundaland show that the Kontum block region is likely moving to the east and rotating clockwise within Sundaland (Chamot-Rooke and Le Pichon, 1999; Chi and Dorobek, 2004; Chi and Geissman, 2013; Cung and Geissman, 2013; Michel et al., 2001; Morley, 2007; Tingay et al., 2010; Tran et al., 2013). This rotation is consistent with a regional model whereby Sundaland is composed of not a rigid core, but instead a continuum rubble of fragments that interact and "jostle" or rotate with respect to one another under regional stresses. The eastward motion of the Kontum block is consistent with a continued overall extrusion of material from the Himalayan collision to the east and southeast. The Da Lat block lacks GPS and paleomagnetic data at a fine enough scale to resolve the proposed southwest-wards motion and merits further investigation (Van Nguyen and Hoai, 2019 and references therein).

6. CONCLUSIONS

Results from remote sensing show a strong NE-SW fault trend for southern Vietnam, with additional, minor N-S, E-W and NW-SE trends. The dominant trend characterized as NE-SW is composed of a dataset dispersed between N and NE orientations, with a peak at the NNE orientation. Many of these lineaments cut basalt flows previously dated at 4.3 ± 0.2 Ma (An et al. 2017) or 0.24 ± 0.1 Ma (Lee et al., 1998), as well as one measured here to be 0.600 ± 0.004 Ma. Fault orientations observed in the field fall into this NE-SW trending class, and are sub-vertical. In the basalt flows (with eruption ages < 5 Ma) these faults have oblique lineations with a strong strike-slip component. In the Jurassic sediments, these faults show two sets of lineations; an older, dip-slip set, and a younger, oblique-slip set.

These results indicate that the NE-SW dominant set of faults cuts basalt flows significantly younger than 5 Ma, and movement on these faults is therefore younger than both the cessation of rifting in the SCS and the cessation of sinistral movement on the Red River Fault. We infer that the NE-SW trending faults cutting the basalt flows are related to the NE-SW trending faults in the Jurassic sediments, and postulate that Jurassic-age dip-slip faults have been reactivated as strike-slip faults post 5 Ma. Strike-slip motion on NE-SW oriented faults is consistent with rotation and extrusion of the Kontum and Da Lat blocks, rather than extension and subsidence, in which case dip-slip (normal) motion would be expected. Furthermore, rotation of the blocks is consistent with continuum rubble behavior of small crustal blocks under the influence of extrusion-driven asthenospheric flow.

7. Acknowledgments. CMB and LJE acknowledge a University of Nebraska-Lincoln College of Arts and Sciences International Partnerships Grant and NSF Grant EAR-1758972. We also acknowledge the OSU Argon Geochronology Lab, particularly Dan Miggins, who made the measurements on the sample

referenced in this paper. Remote sensing data was purchased from Apollo Mapping. Figure 5 was created using this data and VAST maps by Nathan Sorsen as part of an undergraduate research project.

8. REFERENCES

An, A-R., Choi, S.H., Yu, Y., and Le, D-C., 2017. Petrogenesis of Late Cenozoic basaltic rocks from southern Vietnam. Lithos, v. 272-273, p. 192-204.

Bai, L., Iidaka, T., Kawakutsu, H., Morita, Y., and Dzung, N. Q., 2009, Upper mantle anisotropy beneath Indochina block and adjacent regions from shear-wave splitting analysis of Vietnam broadband seismograph array data: Physics of the Earth and Planetary Interiors, v. 176, p. 33-43.

Barckhausen, U., Engels, M., Franke, D., Ladage, S., and Pubellier, M., 2014, Evolution of the South China Sea: Revised ages for breakup and seafloor spreading: Marine and Petroleum Geology, v. 58, p. 599-611.

Briais, A., Patriat, P., and Tapponier, P., 1993, Updated interpretation of magnetic anomalies and seafloor spreading stages in the South China Sea: Implications for the Tertiary tectonics of SE Asia: Journal of Geophysical Research, v. 98, p. 6299-6328.

Calais, E., Dong, L., Wang, M., Shen, Z., & Vergnolle, M. (2006). Continental deformation in Asia from a combined GPS solution. Geophysical Research Letters, 33(24).

Carter, A., Roques, D., and Bristow, C. S., 2000, Denudation history of onshore Central Vietnam: constraints on the Cenozoic evolutio of the western margin of the South China Sea: Tectonophysics, v. 322, p. 265-277.

439 Chamot-Rooke, N., and Le Pichon, X., 1999, GPS determined eastward Sundaland motion with respect to
440 Eurasia confirmed by earthquake slip vectors at Sunda and Philippine trenches: Earth and Planetary
441 Science Letters, v. 173, p. 439-455.

442 Chapple, W. M., & Tullis, T. E. (1977). Evaluation of the forces that drive the plates. Journal of geophysical
443 research, 82(14), 1967-1984.

444 Chi, C. T., and Dorobek, S. L., 2004, Cretaceous palaeomagnetism of Indochina and surrounding regions:
445 Cenozoic tectonic implications, in Malpas, J., Fletcher, C. J. N., Ali, J. R., and Aitchison, J. C., eds., Aspects
446 of the Tectonic Evolution of China, Volume 226: London, Geological Society of London, p. 273-287.

447 Chi, C. T., and Geissman, J., 2013, A review of the paleomagnetic results of Cretaceous rock formations
448 from Vietnam, Indochina and South China, their Cenozoic tectonic implications: Journal of Geodynamics,
449 v. 69, p. 54-64.

450 Chung, S.-L., Cheng, H., Jahn, B., O-Reilly, S. Y., and Zhu, B., 1997, Major and trace element, and Sr-Nd
451 isotope constraints on the origin of Paleogene volcanism in South China prior to the South China Sea
452 opening: Lithos, v. 40, p. 203-220.

453 Clift, P., Lee, G. H., Duc, N. A., Barckhausen, U., Van Long, H., and Zhen, S., 2008, Seismic reflection
454 evidence for a Dangerous Grounds miniplate: No extrusion origin for the South China Sea: Tectonophysics,
455 v. 27, doi: 10.1079/2007TC002216.

456 Cullen, A., Reemst, P., Henstra, G., Gozzard, S., and Ray, A., 2010, Rifting of the South China Sea: New
457 perspectives: Petroleum Geoscience, v. 16, p. 273-282.

458 Cung, T.C. & Geissman, J. W. (2013). A review of the paleomagnetic data from Cretaceous to lower Tertiary
459 rocks from Vietnam, Indochina and South China, and their implications for Cenozoic tectonism in Vietnam
460 and adjacent areas. Journal of Geodynamics, 69, 54-64.

461 Drury, S.A., 2004. Image interpretation in Geology (3rd Ed). Routledge, 304 pp.

462 Duchkov, A. D., Yem, N. T., Toan, D. V., and Bak, C. V., 1992, First estimates of heat flow in Vietnam: Sov.
463 Geol. Geophys., v. 33, p. 92-96.

464 Dung, B. V., Tuan, H. A., Van Kieu, N., Man, H. Q., Thuy, N. T. T., & Huyen, P. T. D. (2018). Depositional
465 environment and reservoir quality of Miocene sediments in the central part of the Nam Con Son Basin,
466 southern Vietnam shelf. Marine and Petroleum Geology, 97, 672-689.

467 Finzel, E. S., Flesch, L. M., and Ridgeway, K. D., 2011, Kinematics of a diffuse North American-Pacific-Bering
468 plate boundary in Alaska and western Canada: Geology, v. 39, p. 835-838.

469 Flower, M. F. J., Tamaki, K., and Hoang, N., 1998, Mantle extrusion: A model for dispersed volcanism and
470 DUPAL-like asthenosphere in East Asia and the Western Pacific, in Flower, M. F. J., Chung, S.-L., Lo, C.-H.,
471 and Lee, T.-Y., eds., Mantle Dynamics and Plate Interactions in East Asia, Volume 27, American
472 Geophysical Union, p. 67-88.

473 Fyhn, M. B. W., Boldreel, L. O., and Nielsen, L. H., 2009a, Geological development of the Central and South
474 Vietnamese margin: Implication for the establishment of the South China Sea, Indochinese escape
475 tectonics, and Cenozoic volcanism: Tectonophysics, v. 478, p. 184-214.

476 Fyhn, M. B. W., Nielsen, L. H., Boldreel, L. O., Thang, L. D., Bojesen-Koefoed, J., Petersen, H. I., Huyen, N.
477 T., Duc, N. A., Dau, N. T., Mathiesen, A., Reid, I., Huong, D. T., Tuan, H. A., Hien, L. V., Nytoft, H. P., and
478 Abatzis, I., 2009b, Geological evolution, regional perspectives and hydrocarbon potential of the northwest
479 Phu Khanh Basin, offshore Central Vietnam: Marine and Petroleum Geology, v. 26, p. 1-24.

480 Fyhn, M. B., Cuong, T. D., Hoang, B. H., Hovikoski, J., Olivarius, M., Tuan, N. Q.,Tung, N.T., Huyen, N.T.,
481 Cuong, T.X., Nytoft, H.P & Abatzis, I. (2018). Linking Paleogene Rifting and Inversion in the Northern Song

Hong and Beibuwan Basins, Vietnam, With Left-Lateral Motion on the Ailao Shan-Red River Shear Zone. Tectonics, 37(8), 2559-2585.

Guo, L., Zhong, Z., Wang, L., Shi, Y. S., Li, H., & Liu, S. W. (2001). Regional tectonic evolution around Yinggehai basin of South China Sea. Geological Journal of China Universities, *7*(1), 1-12.

Gursoy, H., Piper, J. D. A., and Tatar, O., 2003, Neotectonic deformation in the western sector of tectonic escape in Anatolia: paleomagnetic study of the Afyon region, central Turkey: Tectonophysics, v. 374, p. 57-79.

Gursoy, H., Piper, J. D. A., Tatar, O., and Temiz, H., 1997, A palaeomagnetic study of the Sivas Basin, central Turkey: Crustal deformation during lateral extrusion of the Anatolian Block: Tectonophysics, v. 271, no. 89-105.

Hall, R., 2002. Cenozoic geological and plate tectonic evolution of SE Asia and the SW Pacific: computer-based reconstructions, model and animations. Journal of Asian Earth Sciences, v. 20 (4) p353-431.

Hall, R., van Hattum, M., Spakman, W., 2008. Impact of India–Asia collision on SE Asia: the record in Borneo. Tectonophysics, 451 pp. 366-369.

Hennig, J., Breitfeld, H. T., Gough, A., Hall, R., Long, T. V., Kim, V. M., & Quang, S. D. (2018). U-Pb zircon ages and provenance of upper Cenozoic sediments from the Da Lat Zone, SE Vietnam: Implications for an intra-Miocene unconformity and paleo-drainage of the proto–Mekong River. Journal of Sedimentary Research, 88(4), 495-515.

Hoang, N., and Flower, M. F. J., 1998, Petrogenesis of Cenozoic basalts from Vietnam: Implications for origins of a Diffuse Igneous Province: Journal of Petrology, v. 39, p. 369-395.

Huchon, P., Le Pichon, X. and Rangin, C., 1994a. Indochina Peninsula and the collision of India and Eurasia. Geology, v. 22, p. 27-30.

Huchon, P., Le Pichon, X., Rangin, C., and Thi, P.T., 1994b. New marine data from Vietnam Margin limit the amount of extrusion of Indochina during the opening of the South China Sea. AAPG Bull, v. 78.

Kasatkin, S.A., Phach, P.V. Anh, L.D. & Golozubov, V.V., 2017. Cretaceous strike-slip dislocations in the Dalat Zone (Southeastern Vietnam). Russian Journal of Pacific Geology, v. 11 (6) p408-420.

Kuiper, K.F., Deino, A., Hilgen, F.J., Krijgsman, W., Renne, P.R., Wijbrans, J.R. (2008) Synchronizing rock clocks of Earth history, Science v. 325, issue 5875, 500-504. doi: 10.1126/science.1154339.

Lee, T.-Y., Lo, C.-H., Chung, S.-L., Chen, C.-Y., Wang, P.-L., Lin, W.-P., Hoang, N., Chi, C. T., and Yem, N. T., 1998, $^{40}Ar/^{39}Ar$ Dating Result of Neogene Basalts in Vietnam and its Tectonic Implication, *in* Flower, M. F. J., Chung, S.-L., Lo, C.-H., and Lee, T.-Y., eds., Mantle Dynamics and Plate Interactions in East Asia: Washington, DC, AGU, p. 317-330.

Leloup, P. H., Lacassin, R., Tapponnier, P., Schärer, U., Zhong, D., Liu, X., Zhang, L., Ji, S. & Trinh, P. T. (1995). The Ailao Shan-Red River shear zone (Yunnan, China), Tertiary transform boundary of Indochina. Tectonophysics, 251(1-4), 3-84.

Leloup, P.H., Arnaud, N., Lacassin, R., Kienast, J.R., Harrison, T.M., Phan Trong, T.T., Replumaz, A. & Tapponier, P., 2001. New constraints on the structure, thermochronology and timing of the Ailao Shan-Red River shear zone, SE Asia. Journal of Geophysical Research, v. 106, p. 6683-6732.

Lepvrier, C., Maluski, H., Van Tich, V., Leyreloup, A., Thi, P. T., & Van Vuong, N. (2004). The early Triassic Indosinian orogeny in Vietnam (Truong Son Belt and Kontum Massif); implications for the geodynamic evolution of Indochina. Tectonophysics, 393(1-4), 87-118.

Li, C-F., Li, J., Ding, W., Franke, D., Yao, Y., Shi, H., Pang, X., Cao, Y., Lin, J., Kulhanek, D., Williams, T., Bao, R., Briais, A., Brown, E.A., Chen, Y., Clift, P.D., Colwell, F.S., Dadd, K.A., Hernandez-Almeida, I., Huang, X0L., Hyun, S., Jiang, T., Koppers, A.A.P., Li, Q., Liu, C., Liu, Q., Liu, Z., Nagai, R.D., Peleo-Alampay, A., Su, X., Sun,

526 Z., Tejada, M.L.G., Trinh, H.S., Yeh, Y-C., Zhang, C., Zhang, F., Zhang, G-L. & Zhao, X., 2015. Seismic
527 stratigraphy of the central South China Sea basin and implications for neotectonics. Journal of Geophysical
528 Research, v. 120, p. 1377–1399.

529 Liu, H.-L., Yan, P., Zhang, B.-Y., Sun, Y., Zhang, Y.-X., Shu, L.-S., Qiu, X.-L., and Guo, L.-Z., 2004, Role of the
530 Wan-Na fault system in the western Nansha Islands (Southern South China Sea): Journal of Asian Earth
531 Sciences, v. 23, p. 221-233.

532 Mantovani, E., Albarello, D., Babbucci, D., Tamburelli, C., and Viti, M., 2002, Trench-arc-backarc systems
533 in the Mediterranean area: Examples of extrusion tectonics, in Rosenbaum, G., and Lister, G. S., eds.,
534 Reconstruction of the evolution of the Alpine Himalayan Orogen., Volume 8, p. 125-141.

535 Matthews, S.J., Fraser, A. J., Lowe, S., Todd, S.P., & Peel, F.J., 1997. Structure, stratigraphy and petroleum
536 geology of the SE Nam Con Son Basin, offshore Vietnam. In Fraser, A.J., Matthews, S.J., & Murphy, R.W.
537 (eds). Petroleum Geology of SE Asia. Geological Society Special Publication 126, p 89-106.

538 Meng, Q. R., Wang, E., & Hu, J. M. (2005). Mesozoic sedimentary evolution of the northwest Sichuan basin:
539 Implication for continued clockwise rotation of the South China block. Geological Society of America
540 Bulletin, 117(3-4), 396-410.

541 Michel, G. W., Yu, Y. Q., Zhu, S. Y., Reigber, C., Becker, M., Reinhart, E., Simons, W., Ambrosius, B., Vigny,
542 C., Chamot-Rooke, N., Le Pichon, X., Morgan, P., and Matheussen, S., 2001, Crustal motion and block
543 behavior in SE-Asia from GPS measurements: Earth and Planetary Science Letters, v. 187, p. 239-244.

544 Min, K., Mundil, R., Renne, P.R., Ludwig, K.R. (2000) A test for systematic errors in 40Ar/39Ar
545 geochronology through comparison with U/Pb analysis of a 1.1-Ga rhyolite. Geochimica et Cosmochimica
546 Acta, v. 64, issue 1, 73-98. doi: 10.1016/S0016-7037(99)00204-5.

547 Morley, C. K., 2007, Variations in Late Cenozoic-Recent strike slip and oblique-extensional geometries,
548 within Indochina: The influence of pre-existing fabrics: Journal of Structural Geology, v. 29, p. 36-58

549 Morley, C. K. (2012). Late Cretaceous–early Palaeogene tectonic development of SE Asia. Earth-Science
550 Reviews, 115(1-2), 37-75.

551 Nam, T.N., 1995. The geology of Vietnam: A brief summary and problems. Geoscience reports Shizuoka
552 University v22, p1-10

553 Nguyen, T. T. B., Satir, M., Siebel, W., & Chen, F. (2004). Granitoids in the Dalat zone, southern Vietnam:
554 age constraints on magmatism and regional geological implications. International Journal of Earth
555 Sciences, 93(3), 329-340.

556 Pubellier, M., & Morley, C. K. (2014). The basins of Sundaland (SE Asia): Evolution and boundary
557 conditions. Marine and Petroleum Geology, 58, 555-578.

558 Rangin, C., Huchon, P., Le Pichon, X., Bellon, H., Lepyrier, C., Roques, D., Hoe, H. D., and Ouynh, P. V., 1995,
559 Cenozoic deformation of central and south Vietnam: Tectonophysics, v. 251, p. 179-196.

560 Redfield, T. F., Scholl, D. W., Fitzgerald, P. G., and Beck, M. E., Jr., 2007, Escape tectonics and the extrusion
561 of Alaska: Past, present and future: Geology, v. 35, p. 1039-1042.

562 Ridgeway, K. D., and Flesch, L. M., 2007, Cenozoic tectonic processes along the Southern Alaska
563 convergent margin: Geology, v. 35, p. 1055-1056.

564 Savva, D., Meresse, F., Pubellier, M., Chamot-Rooke, N., Lavier, L., Po, K. W., ... & Lamy, G. (2013). Seismic
565 evidence of hyper-stretched crust and mantle exhumation offshore Vietnam. Tectonophysics, 608, 72-83.

566 Searle, M.P., Yeh, M-W., Lin, T-H. & Chung, S-L., 2010. Structural constraints on the timing of left-lateral
567 shear along the Red River shear zone in the Ailao Shan and Diancang Shan Ranges, Yunnan, SW China.
568 Geosphere, v. 6, p. 316-338. DOI: 10.1130/GES00580.1.

569 Shellnutt, J.G., Lan, C.Y., Van Long, T., Usuki, T., Yang, H.J., Mertzman, S.A., Iizuka, Y., Chung, S.L., Wang,
570 K.L. and Hsu, W.Y., 2013. Formation of Cretaceous Cordilleran and post-orogenic granites and their
571 microgranular enclaves from the Dalat zone, southern Vietnam: Tectonic implications for the evolution of
572 Southeast Asia. Lithos, 182, pp.229-241.

573 Simons, W.J.F., Socquet, A., Vigny, C., Ambrosius, B.A.C., Haji Abu, S., Promthong, C., Subarya, C., Sarsito,
574 D.A., Matheussen, S., Morgan, P. and Spakman, W., 2007. A decade of GPS in Southeast Asia: Resolving
575 Sundaland motion and boundaries. Journal of Geophysical Research: Solid Earth, 112(B6).

576 Steiger, R.H. and Jäger, E. (1977) Submission on geochronology: Convention on the use of decay
577 constants in geo- and cosmochronology. Earth and Planetary Science Letters, v. 36, issue 3, 359-362. doi:
578 10.1016/0012-821X(77)90060-7.

579 Swiecicki, T. and Maynard, K., 2009. Geology and Sequence, Stratigraphy of Block 06/94, Nam Con Son
580 Basin, Offshore Vietnam. Proceedings of the 2009 South East Asia Petroleum Exploration Society (SEAPEX)
581 Conference, p. 1-17.

582 Tapponier, P., Peltzer, G., and Armijo, R., 1986, On the mechanics of the collision between India and Asia,
583 in Coward, M. P., and Ries, A. C., eds., Collision Tectonics, Volume 19, p. 113-157.

584 Tapponier, P., Peltzer, G., Le Dain, A. Y., Armijo, R., and Cobbold, P., 1982, Propagation extrusion tectonics
585 in Asia: New insights from simple experiments with plasticine: Geology, v. 10, p. 611-616.

586 Tingay, M., Morley, C., King, R., Hillis, R., Coblentz, D., Hall, R., 2010, Present-day stress field of Southeast
587 Asia, Tectonophysics, v. 482, 92-104.

588 Trần, Đ. T., Nguyễn, T. Y., Dương, C. C., Vy, Q. H., Zuchiewicz, W., & Nguyễn, V. N. (2013). Recent crustal
589 movements of northern Vietnam from GPS data. *Journal of Geodynamics*, *69*, 5-10.

590 Tri, T.V., Khuc, V. (eds)., Tam, B.M., Hoang., C.M., Huyen, D.T., Truong, D.N., Bat, D., Binh, L.D., An, L.D.,
591 Nhuan, M.T, Toan, N.Q., San, N.T., Minh, N.B., Bieu, N., Dy, N.D., Ty, N.H., Hung, N.Q., Van, N.T., Phong,
592 N.T., Quy, N.V., Vuong, N.V., Bao, N.X., Luong, P.D., Ngan, P.K., Thien, P., Trinh, P.T., Phuong, T.H., Nam,
593 T.N., Van, T.T., Thang, T.T., Hai, T.T., Hoa, T.T., Anh, T.T., Long, T.V. & Nghiep, V.C., 2011. Geology and
594 Earth Resources of Vietnam. Ministry of Natural Resources and Environment, General Department of
595 Geology and Minerals of Vietnam, Publishing House for Science and Technology, Hanoi. 645pp

596 Trinh, P.T., Van Liem, N., To, T.D., Van Huong, N., Hai, V.Q., Van Thom, B., Van Phong, T., Vinh, H.Q., Xuyen,
597 N.Q., Thuan, N.V. and Tuc, N.D., 2015. Present day deformation in the east Vietnam sea and surrounding
598 regions. *Vietnam Journal of Marine Science and Technology*, *15*(2), pp.105-118.

599 Uyeda, S., 1994, Heat flow in Vietnam, Circum-Pacific Council Symposium on: Geology, Exploration, and
600 Development Potential of Energy and Mineral Resources of Vietnam and Adjoining Regions. Abstr.
601 Program.

602 Van Nguyen, V., & Hoai, L. T. T. (2019). Cenozoic paleostress evolution in south central Vietnam:
603 Implication for changing dynamics of faulting along the eastern Indochina continental margin. Journal of
604 Asian Earth Sciences, 185, 104006.

605 Wang, Y., Fan, W., Zhang, Y., Peng, T., Chen, X., and Xu, Y., 2006, Kinematics and 40Ar/39Ar geochronology
606 of the Gaoligong and Chongshan shear systems, western Yunnan, China: Implications for early Oligocene
607 tectonic extrusion of SE Asia: Tectonophysics, v. 418, p. 235-254.

608 Yan, P., Deng, H., Liu, H., Zhang, Z., and Jiang, Y., 2006, The temporal and spatial distribution of volcanism
609 in the South China Sea region: Journal of Asian Earth Sciences, v. 27, p. 647-659.

610 Zhou, D., Ru, K., and Chen, H., 1995, Kinematics of Cenozoic extension on the South China Sea continental
611 margin and its implications for the tectonic evolution of the region: Tectonophysics, v. 251, p. 161-177.

612 Zhu, M., Graham, S. and McHargue, T., 2009. The red river fault zone in the Yinggehai Basin, South China
613 Sea. Tectonophysics, 476(3-4), pp.397-417.

614 Zuchiewicz, W., Quốc Cu'ò'ng, N., Zasadni, J., & Yêm, N. T. (2013). Late Cenozoic tectonics of the Red River
615 Fault Zone, Vietnam, in the light of geomorphic studies. Journal of Geodynamics, 69, 11-30.

616

617 **Table 1**

Location #	Latitude (°N)	Longitude (°E)	Elevation (ft)	Brief field description
1	11.4091	107.6399333	788	Quarry in Dambri town, in Jurassic sediments; faulted
2	10.9964	107.1432833	864	Quarry in Soc Lu Formation – basaltic andesite; faulted
3	10.87686667	107.2284	841	Old quarry in alkali basalt; faulted
4	10.38025	107.2564	6	Cretaceous granite outcrop on the coast near Vung Tau; Ca Na-Vung Tau fault zone prominent
5-7	10.38073333	107.2524667	3	Cretaceous granite outcrops on the coast near Vung Tau; subsidiary fault systems to Ca Na-Vung Tau fault zone

8	10.50761667	107.2729167	229	Alkali basalt quarry with xenoliths; jointed but not faulted.

618

619 Table 1: Co-ordinates and brief field descriptions for the locations referenced in this study. Co-ordinates
620 are given in decimal degrees and in WGS 84 convention. Elevations are given in feet above sea level.

621

622

623

624

625

626

627

628

629

630

631

632

633

634

Figure 1

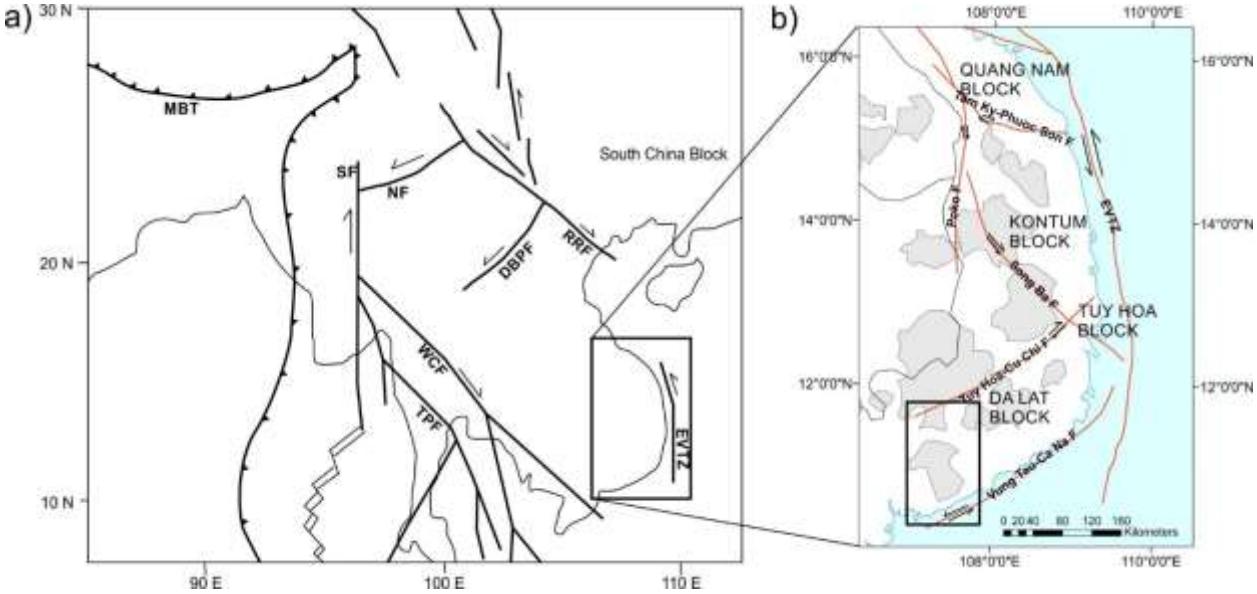

Tectonic maps of the region. a) shows regional faults of the Himalayan orogen as well as the major strike-slip faults of the Indochina Peninsula, modified after Leloup et al. (1995) and Nam (1995). MBT, Main Boundary Thrust; SF, Sagaing Fault; NF, Nanting Fault; TPF, Three Pagodas Fault; WCF, Wang Chao Fault; EVTZ, East Vietnam Transfer Zone; RRF, Red River Fault; DBPF, Dien Bien Phu Fault. b) Block map of the wider study area after Kasatkin et al. (2017). Red lines mark faults, grey areas are volcanic centers. Black box marks the present detailed study area.

Figure 2:

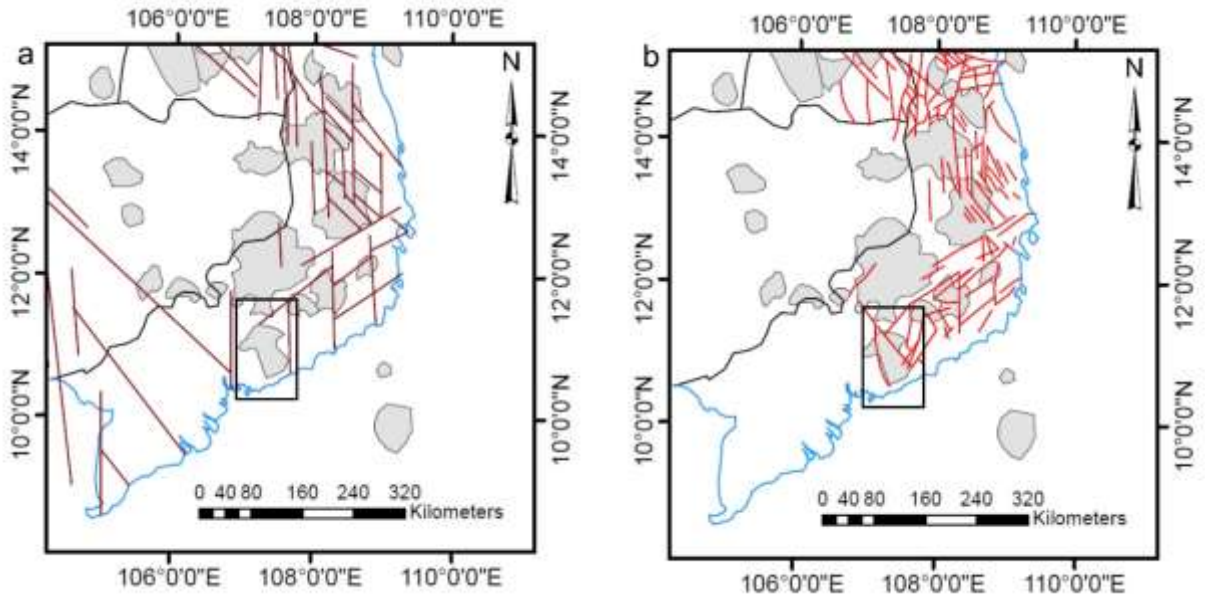

Contrasting fault maps for the Da Lat block and southern part of the Kontum block. a) is from Huchon et al. (1994a), and shows their interpretation of the Paleogene fault framework in the region. b) is from Rangin et al. (1995) and shows their contrasting interpretation of the dominant fault patterns in the area. Grey areas are volcanic centers and the black box marks the location of the present study area.

675 Figure 3:

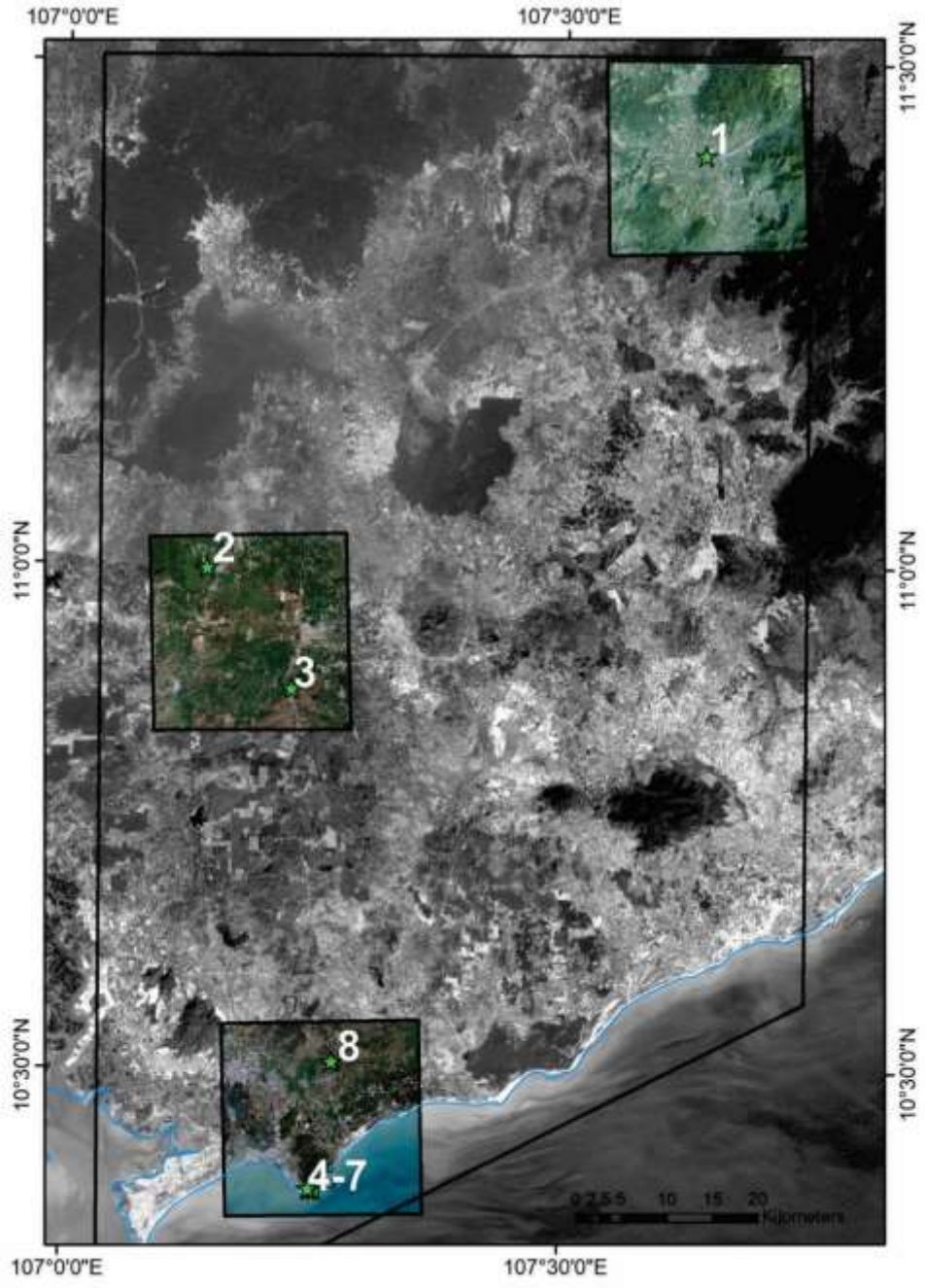

676

677 Landsat ETM+ coverage of the study area, in greyscale, showing field locations (green stars with white
678 numbers) and locations of the SPOT patches used for detailed analysis of key areas (colored squares of
679 higher resolution imagery).

680

681

682

683 Figure 4:

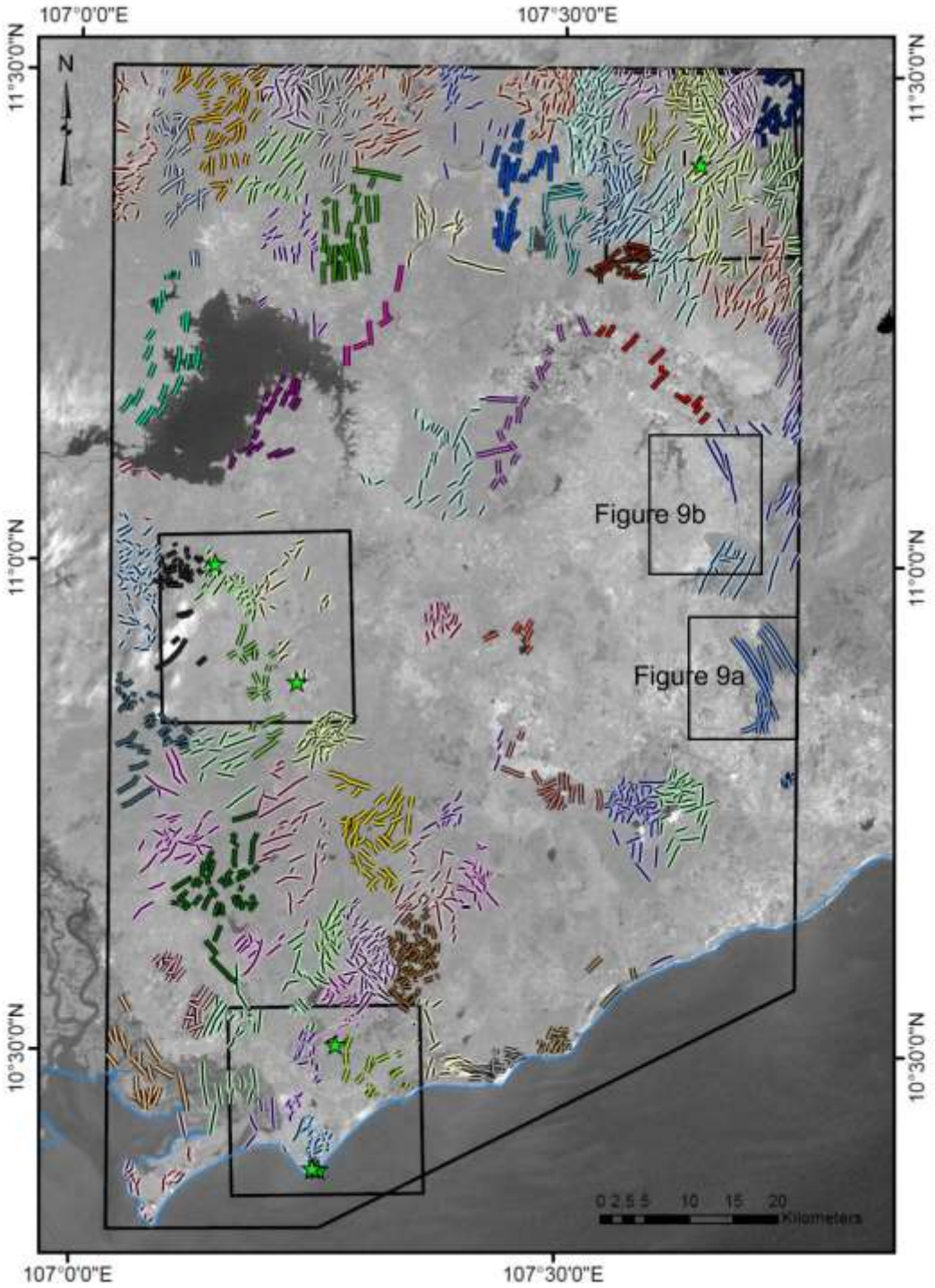

684

685 Classified lineaments across the study area, superimposed on a Landsat ETM+ image. Lineaments have
686 been classified into 75 bins based on a nearest neighbor algorithm in the ArcGIS Grouping Analysis. Black
687 boxes show the location of SPOT datasets. Green stars represent the locations visited in the field, with
688 location numbers as in Figure 3. The location of Figure 13a and Figure 13b are also shown.

689 Figure 5

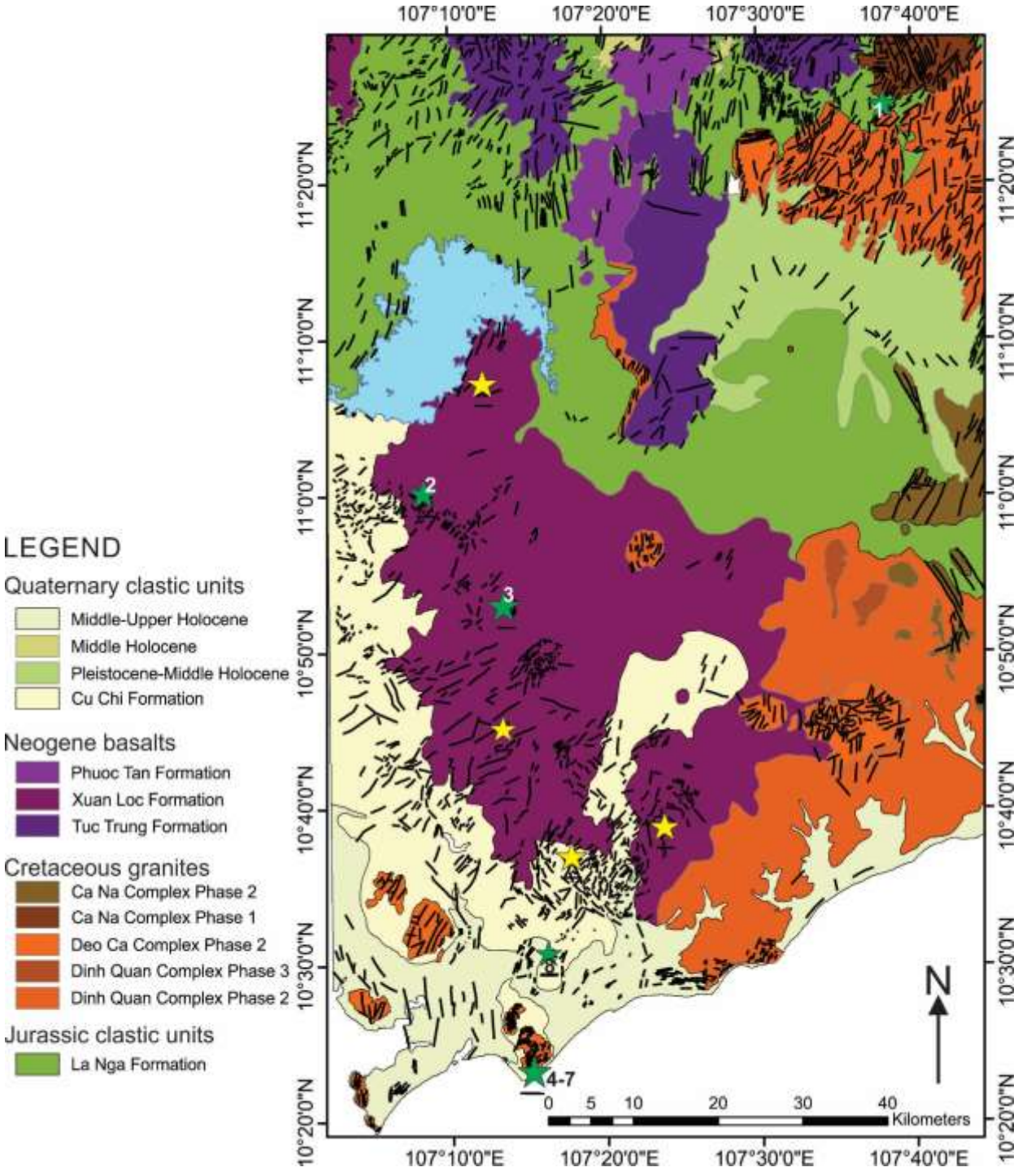

690

691 Geologic map of the study area showing that lineaments cut both young (Neogene) and older
692 (Cretaceous-Jurassic) formations. Numbered green stars mark field locations from this study. Yellow
693 stars mark locations with previously dated basalts (either from outcrop or from core) from Lee et al.
694 (1998) ranging in age from 2.42 ± 0.08 Ma in the south, to 0.24 ± 0.06 Ma in the north of the Xuan Loc
695 Formation. Basalts at location 2 have been previously dated by An et al. (2017) to be 4.3 ± 0.2 Ma.

Figure 6

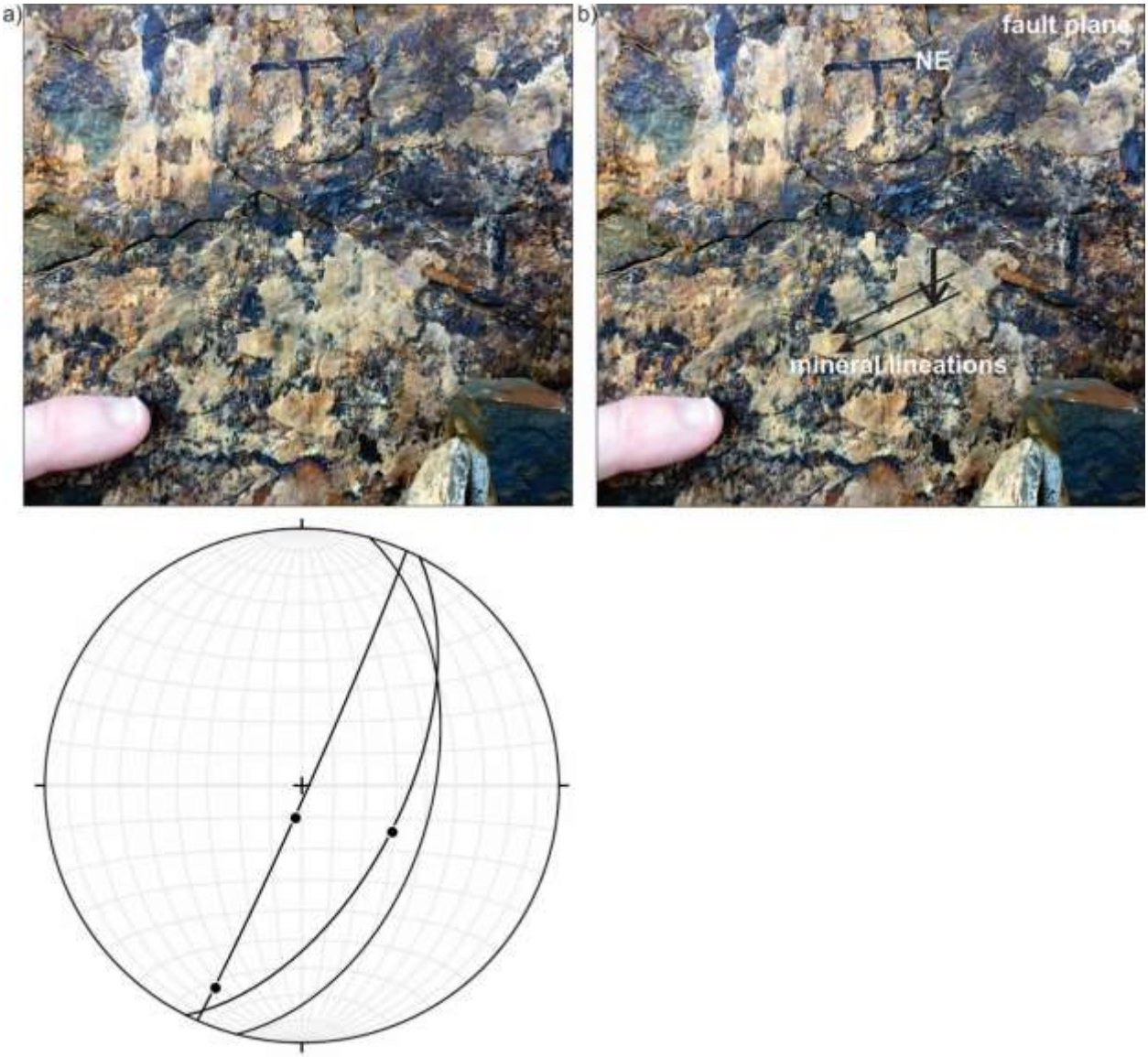

a) Field photograph showing fault plane with mineral lineations in the Jurassic sediments at location 1. b) Annotated version of image in part (a); black arrows show orientations of mineral lineations, where the longer arrows cross-cut the shorter, dip-slip arrow. c) stereonet with great circles indicating fault planes, and dots indicating lineations on fault planes where observed. The stereonet shows all faults present at this location. The near-vertical fault plane with two lineations is the fault plane shown in parts a and b.

Figure 7

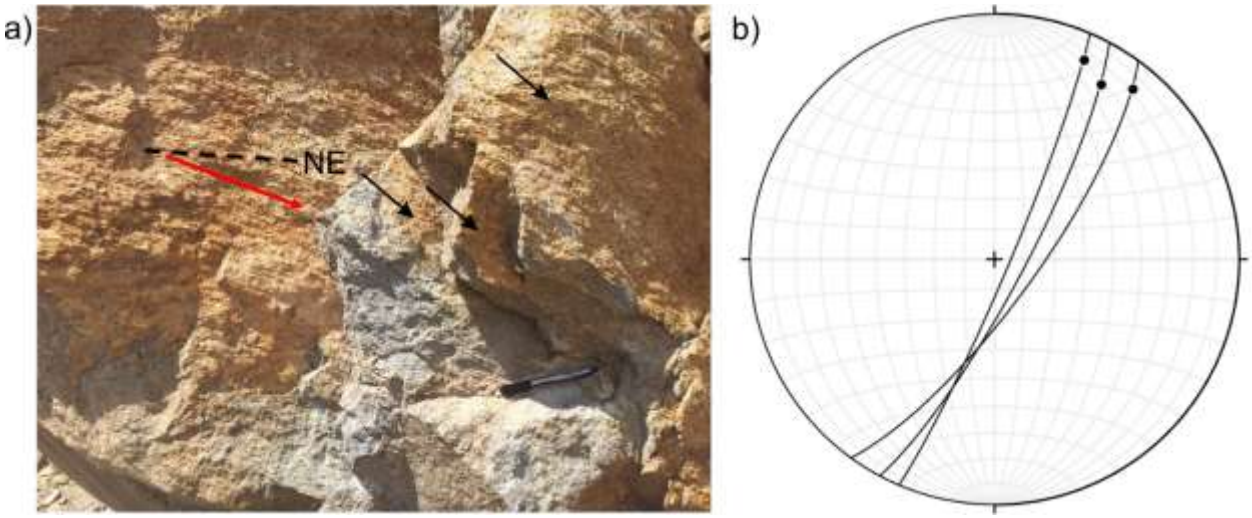

a) Faults in the Pliocene Soc Lu Formation, at location 2. The black dashed line shows the strike of the fault, and the red arrow shows the trend and plunge of the lineations on one fault plane. Other fault planes are arrowed. b) Stereonet as for Figure 6, showing fault planes and lineations recorded at this location. Note the lack of dip-slip lineations and the prevalence of strike-slip lineations.

730 Figure 8

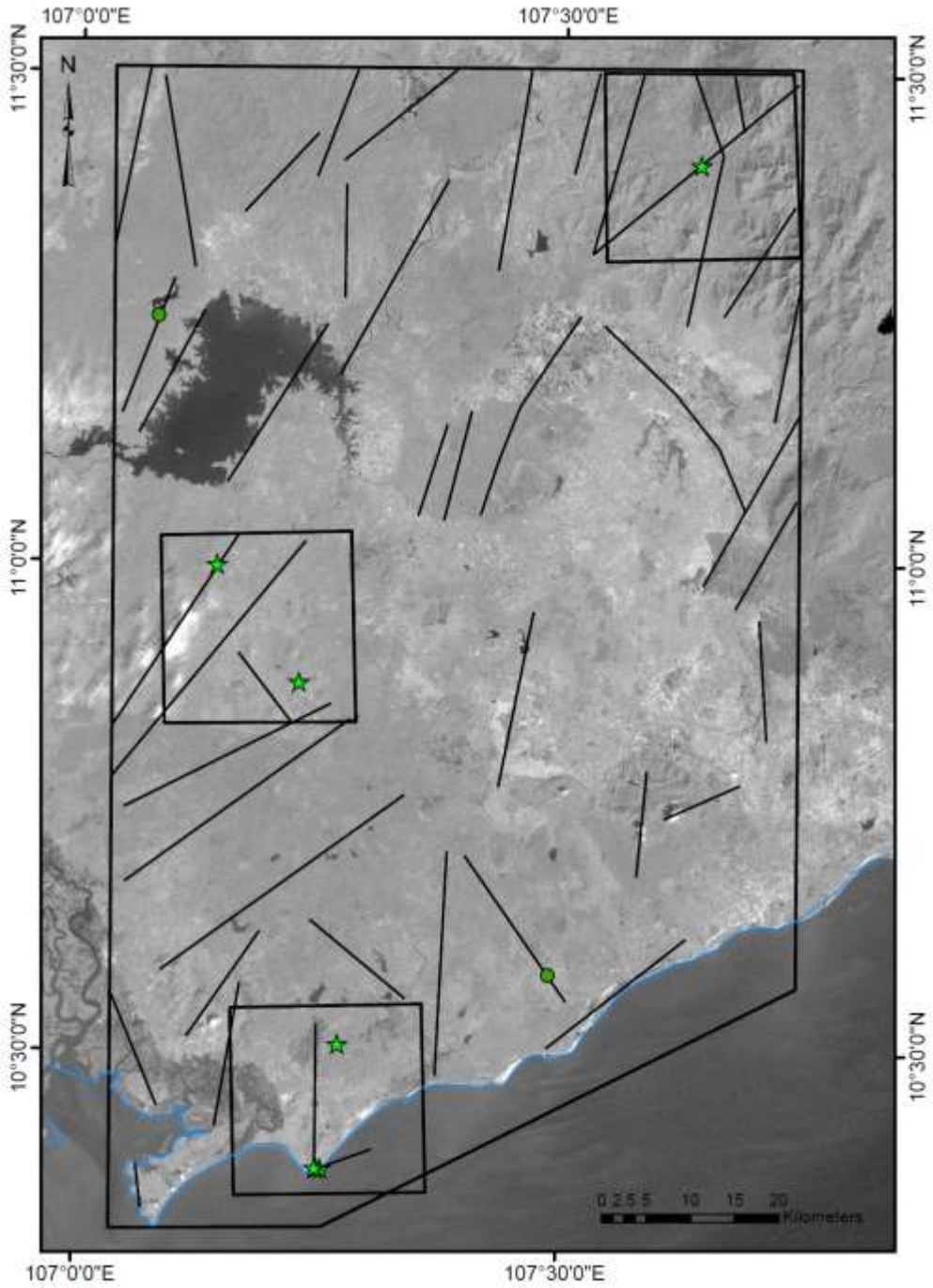

731

732 Post-Jurassic, pre-Neogene fault map of the study area, derived from the classified lineaments. Black
733 boxes show the location of SPOT datasets. Green stars represent the locations visited in the field, with
734 location numbers as in Figure 3. Green dots represent the locations of known earthquakes.

735

736

737 Figure 9

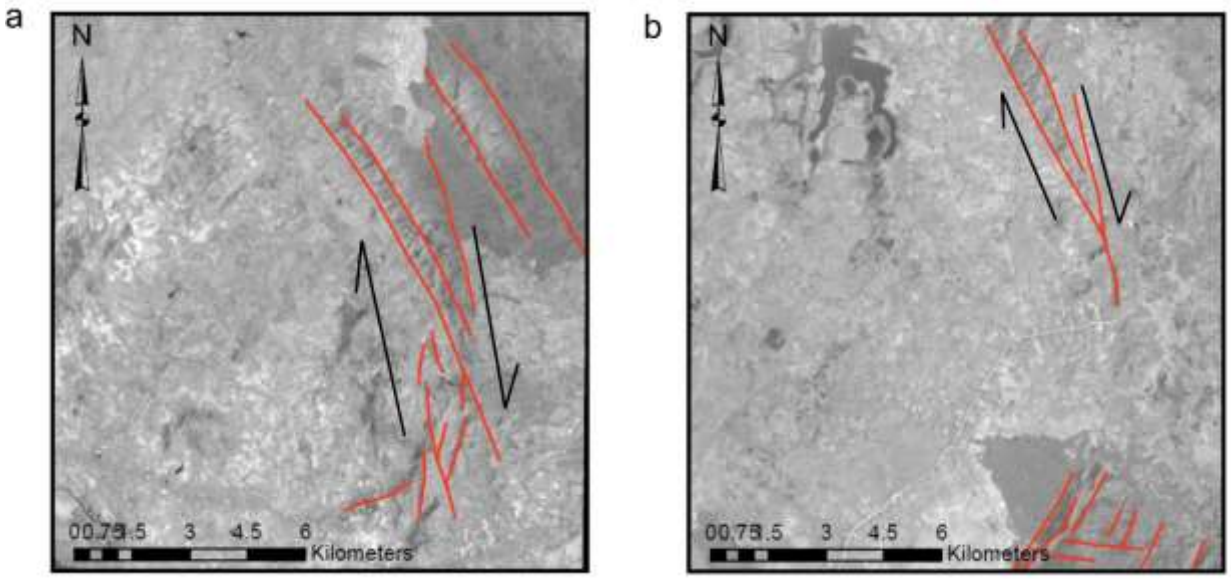

738

739 Examples of lineament patterns developing above a reactivated strike slip fault. For the location of each
740 of these examples, see Figure 4.

741